Fabrication and Characterization of Self-Assembled Nanoparticle/Polyelectrolyte Multilayer Films

ARTICLE *in* THE JOURNAL OF PHYSICAL CHEMISTRY B · NOVEMBER 2003

Impact Factor: 3.3 · DOI: 10.1021/jp035388+

ARTICLES

Fabrication and Characterization of Self-Assembled Nanoparticle/Polyelectrolyte Multilayer Films

Nicola E. Cant, Hao-Li Zhang, Kevin Critchley, Tetyana A. Mykhalyk, Geoffrey R. Davies, and Stephen D. Evans*

Department of Physics and Astronomy, University of Leeds, Leeds LS2 9JT, U.K.

Received: May 20, 2003; In Final Form: August 26, 2003

The formation of multilayer films of organothiol-stabilized gold nanoparticles and polyelectrolyte, synthesized using the "layer-by-layer" technique, has been investigated. The formation of such films requires the alternation of surface charge with each layer deposited and is thus amenable to study by the Kelvin probe technique. The early stages of multilayer film formation have been studied using a combination of X-ray photoelectron spectroscopy, spectroscopic ellipsometry, and Kelvin probe microscopy. Our results suggest that the polyelectrolyte/nanoparticle film can be considered as a wide-band-gap semiconductor with a depletion width, at the substrate/film interface, extending several nanometers into the film. From our ellipsometry data, we are able to provide optical constants for these hybrid organic/inorganic films.

Introduction

With the increasing demand for ever smaller devices, much recent research has focused on the fabrication and characterization of "self-organizing" nanoscale systems. This shift away from "top-down" approaches, such as those based on photolithography, to a "bottom-up" approach should not only permit the fabrication of much smaller devices but also allow facile, and yet highly reproducible, assembly. Nanoparticles represent an interesting class of materials whose properties lie somewhere between those of individual atoms or molecules and those of bulk materials. These particles are of interest for several reasons: First, it is possible that new energy levels become available because of the reduced dimensionality of the system; this is particularly relevant to semiconductor particles.[1] For metallic nanoparticles, it is not so much that the energy levels change but rather that the reduced dimensions of the particles become smaller than the electron mean free path. This leads to increased electron scattering and, hence, affects both the electronic and optical properties of the nanoparticles. Further, by reducing the size of such particles, one also reduces the capacitance associated with charging them, which, in turn, can lead to interesting conductivity behavior, for example, room-temperature single-electron transport.[2,3] Finally, on reducing the dimensions of a particle, one implicitly increases the surface-area-to-volume ratio, which might be of considerable interest in catalysis and biolabeling.

The work described here is focused on the early stages of multilayer film formation of alternate gold-nanoparticle/polyelectrolyte layers. The method by which multilayer films of this type are formed was pioneered by Iler[4] and later by Decher[5] and relies on electrostatic interactions between alternate layers of opposite charge, as well as a contribution from dispersive interactions. Many different materials have been used in the synthesis of multilayer films, with the only apparent requirement being that the components should be of opposite net charge. This flexibility has led to a variety of different substances, from biological macromolecules to polyelectrolytes[5−7] and metallic nanoparticles, all being used in such films. The technique should also allow films of multiple components to be produced, provided that neighboring layers are of opposite charge, although, to our knowledge, only two- and three-component systems have been studied to date.

A number of studies have been performed specifically investigating the buildup of nanoparticle/polyelectrolyte composites, with many different combinations of materials possible. Some common nanoparticle components in these films have been SiO_2,[8,9] TiO_2,[10,11] iron oxide,[12] and gold.[13] These materials have been combined with polymers such as poly(styrene sulfonic acid),[10,12] poly(allylamine hydrochloride), and poly(diallyldimethylammonium chloride).[8,11,12] To date, a significant amount of the work has focused on illustrating the regular formation of these films by UV/visible spectroscopy,[10,13−16] because the growth of the plasmon absorption band with nanoparticle concentration is an easy feature to monitor. These papers generally report an anomalous initial growth, followed by a regime where regular multilayer buildup occurs.[15−18]

The alternation of surface properties during "layer-by-layer" growth has been demonstrated with zeta potential and contact angle measurements.[10,18,19] Further, Li et al. have used the Kelvin probe technique to illustrate the alternation of surface charge for the layer-by-layer deposition of organic molecules.[20−22] In the work presented here, the Kelvin probe technique is used to follow multilayer film growth of polyelectrolyte/nanoparticle systems. In particular, we concentrate on the early stages of film deposition where these systems demonstrate a crossover from anomalous to regular layer-by-layer growth. X-ray pho-

* Corresponding author. E-mail: s.d.evans@leeds.ac.uk.

10.1021/jp035388+ CCC: $25.00
Published on Web 11/05/2003

toelectron spectroscopy (XPS) is not generally used as a tool to characterize film, as typical film thicknesses exceed the escape depth of the photoexcited electrons. However, for the thin films under investigation here, XPS can be used as a monitor of film growth, as well as a source of information on film composition. Finally, by combining UV/visible spectroscopy data with data obtained from variable-angle spectroscopic ellipsometry, we are able to determine the optical constants (n k) for the nanoparticle/polyelectrolyte systems.

Experimental Section

Materials. 4-Mercaptobenzoic acid, sodium borohydride, hydrogen peroxide (27.5 wt % solution in water), (3-aminopropyl)-triethoxysilane (APTES), and poly(diallyldimethylammonium chloride) (PDDA, 20 wt % solution in water, molecular weight 200 000−350 000) were all used as received from Aldrich. Sulfuric acid (98%) was supplied by Fisher Scientific, and hydrogen tetrachloroaurate trihydrate(III) ($HAuCl_4$) was supplied by Alfa Aesar; both were used as received. All water was Millipore Milli-Q grade with a resistivity better than 18 MΩ cm. Silicon substrates were cut from n-type doped (100) wafers, with a resistivity of 1−5 Ω cm, supplied by Laporte Electronics.

Nanoparticle Formation. 4-Mercaptobenzoic acid stabilized gold nanoparticles (Au:COOH) were prepared by the reduction of $HAuCl_4$ with sodium borohydride in the presence of the stabilizing material as previously described.[23] This method results in the formation of predominantly uncharged particles distributed in methanol. The stabilizing ligand binds to the gold through the formation of a thiolate bond, leaving carboxylic acid groups exposed at the surface.

For the purpose of multilayer film formation using the layer-by-layer technique, the particles should be charged. This is achieved by exchanging the solvent; the particles are dissolved in Millipore water, and the pH is adjusted with $NaOH_{(aq)}$ such that it is greater than 10. For aqueous solutions with pH > 10, the carboxylic acid group should be completely dissociated, thus leaving the nanoparticles negatively charged.[23]

Substrate Cleaning. Prior to silanization, the silicon substrates were thoroughly cleaned by sequential ultrasonication in methanol, dichloromethane, and methanol, each for 15 min. The substrates were then dried under a stream of nitrogen before being immersed in piranha solution (70:30, v/v, H_2SO_4/H_2O_2) for approximately 15 min.*Caution: Piranha solution reacts violently with organic materials and must be handled with great care.*) Finally, substrates were thoroughly rinsed with Millipore water. The cleaned substrates were used within 2 h, during which they were stored under Millipore water. This method of cleaning should leave the silicon surface smooth, hydrophilic, and hydroxylized and therefore appropriate for organosilane deposition.[24]

Surface Functionalization. Substrates were functionalized with the aminosilane APTES to produce a positively charged surface.[25] A 10% solution of APTES in toluene was passed through a 0.2-μm filter before the substrates (thoroughly dried under a stream of nitrogen) were introduced. The system was kept under a nitrogen atmosphere (to avoid the excessive uptake of water) at room temperature for a period of 1 h. Next, the substrates were removed from the silane solution and washed, by ultrasonication for 2 min, in toluene and then dichloromethane.

All samples remained under dichloromethane for a time period not exceeding 7 h until use. Immediately prior to use, the samples were removed from the final washing solvent, dried in nitrogen, and rinsed under a stream of Millipore water for 2 min.

Multilayer Film Deposition. Multilayer films were deposited using a home-built automated dipping machine. This device slowly lowered and raised samples from the appropriate solutions at a constant speed, ensuring maximum reproducibility of the dipping technique. Substrates were held at their base with a small, custom-made stainless steel clamp that had been previously cleaned in dichloromethane.

Substrates were first dipped into an aqueous solution of Au:COOH (pH > 10) for 600 s. They were then immersed in a beaker of fresh Millipore water for 10 s to remove excess material before being immersed in a 1% aqueous solution of PDDA for 600 s. Finally, the washing process was repeated to complete the deposition of a full bilayer. The bilayer deposition process was repeated until the required number of layers had been formed.

An accurate concentration of the nanoparticle solution was not known; however, the concentration was held constant through monitoring of the intensity of the surface plasmon absorption band at 530 nm.

Characterization. The surface potential of each sample was measured using a home-built Kelvin probe apparatus. This consisted of a sample stage with $x-y$ motion and a vibrating probe (area = 2.7 mm^2) that was lowered toward the sample until a separation of approximately 20 μm was achieved. During this time, the probe was oscillated at a frequency of 800 Hz, driven by a piezo actuator, P200-16, supplied by Linos Photonics. The alternating current generated by the oscillation of the tip−sample separation was measured using a lock-in amplifier (Perkin-Elmer Instruments model 7220). The application of a dc bias equal in magnitude to the contact potential difference but of opposite sign allowed the "nulling" of the ac signal. Five readings per sample were taken, each in different regions, to ensure that the readings were representative of the sample.

UV/visible absorption spectra were obtained with a Shimadzu UV-2101PC spectrometer fitted with a reflectance kit to enable the collection of spectra from samples on silicon. The slit width was set to 0.1 nm, and scans were collected on the "very slow" setting (less than 4 nm/min with a step size of 0.05 nm) over the range 400−750 nm.

Spectroscopic ellipsometry was carried out on a Beaglehole Instruments picometer ellipsometer. Variable-wavelength scans (400−750 nm) were performed at three separate angles, 65°, 70°, and 75°. Variable-angle scans (70−80°) were done at a wavelength of 633 nm. Fitting was performed by separating the multilayer film system into three parts, substrate, silane, and nanoparticle/polyelectrolyte film.

XPS spectra were obtained using a Vacuum Generators ML500 spectrometer with a chamber pressure maintained at $<10^{-8}$ Torr. A 250-W unmonochromated Al Kα X-ray source was used to irradiate the samples, and the pass energy of the analyzer was set to 30 eV. Spectra were obtained with an electron takeoff angle of 90° to ensure that the full depth of the sample was probed. High-resolution spectra were fitted, where appropriate, with a pseudo-Voigt function.[26]

Results and Discussion

Gold nanoparticles were formed as described in the Experimental Section above. These particles were characterized using UV/visible and FT-IR spectroscopy, as well as transmission electron microscopy (TEM). The size distribution of the nanoparticles was found through analysis of TEM images of particles distributed on carbon-coated copper grids. From a

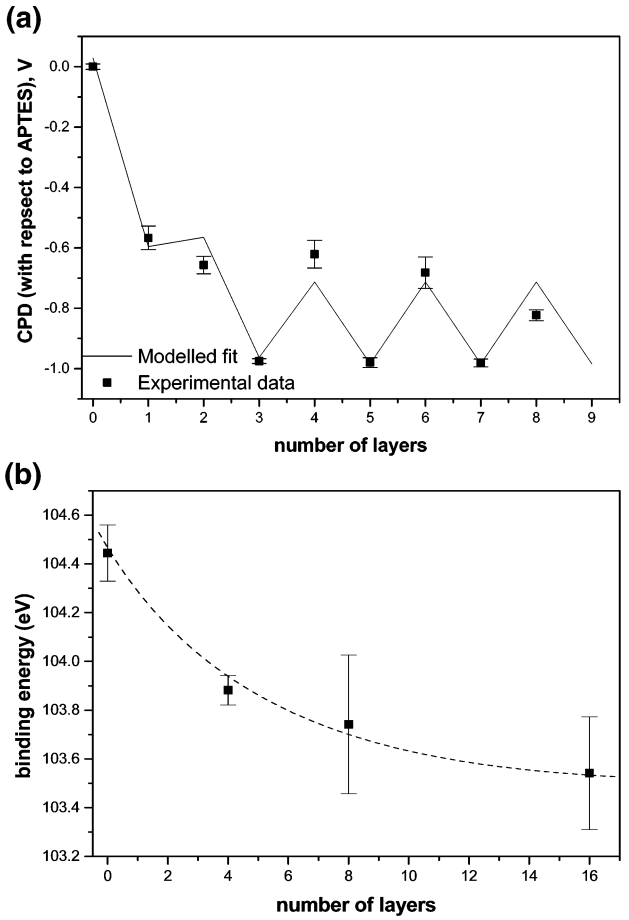

Figure 1. (a) Contact potential difference (CPD) for multilayer films consisting of alternate layers of Au:COOH and PDDA, deposited on an APTES-functionalized silicon support. The CPD values presented are relative to those obtained for the APTES-derivatized substrate. The solid squares represent experimental data, and the line corresponds to a model (see text). The clear alternation of the contact potential difference indicates the oscillation of the surface charge with each layer deposited. Each experimental data point represents the average of readings taken on multiple samples. (b) XPS peak position for the Si 2p peak at 104 eV as a function of the number of layers for even-numbered layers. Each point is the average of data collected from four samples, and the dashed line is a guide to the eye.

histogram of frequency versus particle size, a mean particle size of 5 ± 1 nm was calculated.

UV/visible spectroscopy of the nanoparticles in solution showed a plasmon absorption band centered around 530 nm, which is consistent with the size of nanoparticles produced here.[23] The presence of the stabilizing ligand was evident in the FT-IR spectra of samples in KBr pellets.

Multilayer films were constructed via the sequential deposition of the acid-functionalized nanoparticles (Au:COOH) and the polyelectrolyte (PDDA). The process was performed with a home-built automated dipping machine to regulate the formation and with typical immersion times of 600 s. This immersion period falls within the range of adsorption times typically quoted in the literature, which span from 20 s to several hours.[15,16,27−31] Nanoparticle content and film structure have been previously reported for very thin films using AFM and XPS.[25]

The Kelvin probe technique provides information regarding the contact potential difference (CPD) between two surfaces. This makes it extremely sensitive to the introduction of charge or the presence of adsorbates, e.g., a self-assembled monolayer. Given that the method of multilayer formation is based on

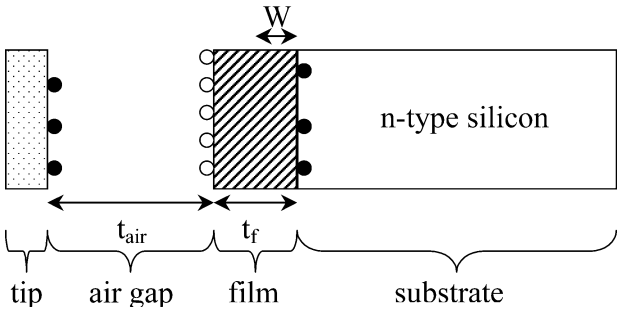

Figure 2. Schematic showing the simplified layer structure used to model the CPD results. The black and white circles represent charges of opposite sign, where white dots are the charge of the uppermost film layer and black dots are the charge induced at the tip and substrate surfaces.

electrostatic interactions between successive layers yielding complete surface charge reversal, the Kelvin probe technique is ideal for following multilayer film formation.

In the discussion of results, the base layer is taken as APTES-functionalized silicon, layer 1 and subsequent odd-numbered layers correspond to the deposition of Au:COOH nanoparticles while layer 2 and subsequent even-numbered layers correspond to the deposition of PDDA.

The variation in contact potential difference (CPD) during the early stages of multilayer film formation is shown in Figure 1a. The APTES SAM used as the baseline for comparing subsequent layer deposition was positively charged and gave a CPD of +1250 mV with respect to clean silicon. Following the deposition of the first layer, consisting of negatively charged nanoparticles, the CPD decreased by ~600 mV. Surprisingly, the addition of the second layer, positively charged APTES, led not to an increase in the CPD but to a slight decrease. Subsequent layers led to an alternation of the CPD values between −1000 and −700 mV for nanoparticles (odd-numbered layers) and polyelectrolyte (even-numbered layers), respectively. In this regime, we consider surface charge reversal to be the dominant contribution to the CPD.

To explain the anomalous behavior observed in the first few layers, we considered the nanoparticle/polyelectrolyte film to behave as a wide-band-gap semiconductor. Thus, in addition to the contribution to the CPD from charge reversal, we must include a second contribution arising from the equilibration of the Fermi levels between the highly doped n-type silicon substrate and the deposited film.[21] For very thin films, however, the dopant density is insufficiently large to achieve equilibration, and the band bending is essentially "frustrated". Once the film thickness has increased to a value greater than the depletion width of the film, the contribution from the built-in potential remains constant, and only that due to charge reversal leads to changes in the CPD value.

To aid our interpretation, we created a model from which predictions of the variation in the CPD can be obtained. The simplest such model assumes a relatively conducting substrate (highly doped Si) onto which has been deposited a relatively insulating layer (the film comprising Au:COOH/PDDA layers on top of APTES) above which an air gap exists between the film and the conducting metal tip of the Kelvin probe (Figure 2).[32]

Assuming that the film can be considered electrically neutral except for the outermost layer, which will carry either a positive or negative charge depending on whether it consists of PDDA or nanoparticles, respectively, then the CPD contribution from this layer of charge is simply given by

$$V_Q = \frac{Q}{C_{film}} - \frac{Q}{C_{air}} = \frac{Qt_{film}}{\epsilon_r\epsilon_0 A} - \frac{Qt_{air}}{\epsilon_0 A} = \frac{(-1)^n|\rho|t_{film}}{\epsilon_r\epsilon_0} - \frac{(-1)^n|\rho|t_{air}}{\epsilon_0} \quad (1)$$

where ρ ($= Q/A$) is the surface charge per unit area, t is the thickness of the layer, ϵ_r is the relative permittivity of the film, and $\epsilon_0$is the permittivity of free space.[32,33] The introduction of the $(-1)^n$ term in eq 1 is to account for the oscillatory nature of the sign of the charged layer present at the surface of the multilayer film, where n is the number of layers deposited.

If the multilayer film is considered as a wide-band-gap semiconductor, then following film formation, the Fermi levels of the two media are brought into coincidence through electron transfer. Assuming a low acceptor/donor density in the multilayer film, one would expect the majority of depletion to occur across the multilayer film as opposed to the heavily doped silicon substrate, thus allowing the system to be treated, as a first approximation, as an abrupt junction. The band bending contribution for an abrupt junction is given by[32−34]

$$-\frac{\partial^2 V}{\partial x^2} = \frac{\rho(x)}{\epsilon_r\epsilon_0} = \frac{qN_D}{\epsilon_r\epsilon_0} \quad (2)$$

where q is the charge of the dopant, V is the potential, ϵ_0 is the permittivity of free space, ϵ_r is the relative permittivity of the material in which the band bending occurs, and N_D is this material's doping density. The sign of q is dependent on the type of material in which band bending is occurring, positive for an n-type semiconductor and negative for a p-type. Integrating this expression with respect to x (the distance from the junction) and applying the boundary condition that $E = 0$ for $x \geq W$, we find that, for a p-type material, the electric field, E, is given by[33]

$$E = \frac{-qN_D}{\epsilon_r\epsilon_0}(x - W) \quad (3)$$

where, for an abrupt junction, W is the distance from the junction over which band bending occurs. Integrating eq 3 with respect to x, we can obtain equations for the built-in potential, as a function of x, that describes the band bending

$$V_{BI}(x) = E_m\left(x - \frac{x^2}{2W}\right) \qquad \text{for } x < W \quad (4a)$$

$$V_{BI}(x) = \frac{1}{2}E_m W \qquad \text{for } x \geq W \quad (4b)$$

where E_m is the value of the field at $x = 0$. Therefore, by combining eqs 1 and 4, we find that the CPD is given by[32]

$$V_{CPD} = V_{BI} + V \quad (5)$$

$$V_{CPD} = V_{BI} + \frac{\rho(-1)^n}{\epsilon_0}\left[\frac{nt_l}{\epsilon_r} - t_{air}\right] \quad (6)$$

where V_{BI} is given by eqs 4 above. The film thickness, t_{film}, is given by the number of layers, n, multiplied by the thickness of each layer, t_l, while the tip−sample separation is given by t_{air} and the relative permittivity of the film by ϵ_r.

To apply eq 6, values for the various parameters were taken as follows: t_{air} was set equal to 20 μm, while ϵ_r and t_l were determined from the ellipsometric data discussed later, with t_l estimated to be 0.65 nm. The value for ϵ_r was determined from the real part of the square of the complex refractive index of the film at 633 nm, which was found to be 2.96. Because no values for ρ, W, and N_D were readily available, these parameters were varied to determine the best fit to the data.

The values found for N_D, ρ, and W that best fitted the experimental data (Figure 1a) were as follows: $N_D = 4.4 \times 10^{25}$ m^{-3}, $\rho = 6.0 \times 10^{-8}$ C m^{-2}, and $W = 3.0 \times 10^{-9}$ m. With the film modeled as a p-type material, i.e., with negatively charged dopants, the magnitude and direction of the band bending found in the experimental data were obtained, suggesting that the Au:COOH/PDDA multilayer film behaves as a p-type semiconductor. We note that the deviation from regular oscillatory behavior at low layer number comes naturally from this model without the need to invoke differences in film structure.

If the CPD were to slowly converge toward the midpoint of the oscillation, then a juncture would be reached above which no reversal of the surface charge occurred, thus effectively halting the adsorption of subsequent layers. Such behavior was not observed in our experimental work nor in that reported in the literature.[35]

XPS was used to follow multilayer film formation to evaluate both the composition and uniformity of the film. In addition to this information, however, we also observed a systematic variation in the peak positions as a function of layer number. In particular, we found that the peak shifts mirrored the trends observed with the Kelvin probe technique. Figure 1b illustrates the shift in binding energy of the Si − O peak (~104 eV) as a function of the number of layers. The deposition of APTES resulted in a shift of this peak to a binding energy higher than that expected for the natural oxide on the silicon surface, indicating the increased net positive surface charge. However, the addition of subsequent bilayers caused the peak to shift to lower binding energy, indicating a decrease in work function possibly associated with the band bending measured with the Kelvin probe technique (Figure 1a).

Survey spectra of the APTES-functionalized silicon substrate typically showed the presence of silicon (with contributions from the substrate and the adsorbed silane), oxygen, carbon, and nitrogen. High-resolution scans (not shown) of the Si 2p region showed the presence of two bands at 100 and 104 eV corresponding to bulk silicon and to the silane, respectively. The addition of a nanoparticle layer gave rise to the appearance of gold and sulfur signals in the survey spectra in addition to those seen for the APTES-functionalized silicon. The Au 4f peaks occur at 85 and 89 eV, while the weak S 2p doublet is situated at 164 eV. The subsequent adsorption of PDDA resulted in an increase in the N 1s signal (binding energy $\approx$ 400 eV). The change in intensity of these peaks was used to monitor the layer-by-layer growth.

Figure 3 shows the variation in integrated intensity of the N 1s and Au 4f signals as a function of the number of layers deposited. It is evident that both the PDDA and the nanoparticle layers increase approximately linearly with increasing layer number. The error bars correspond to the uncertainty associated with each point and indicate that the uncertainty increases with the number of layers. This increase in uncertainty reflects the fact that small variations in the quality of the initial layers are effectively magnified during multilayer growth. Further, the first nanoparticle layer appears to have a higher coverage than subsequent nanoparticle layers, suggesting a difference in surface charge density between the APTES SAM and subsequent

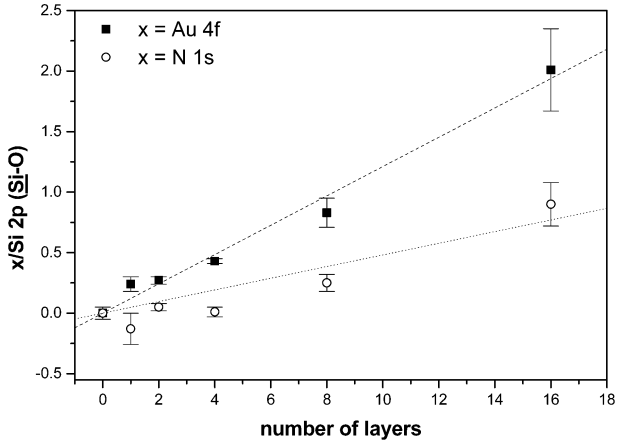

Figure 3. Ratio of film components as determined by XPS for multilayer films of Au:COOH and PDDA on APTES-functionalized silicon. The Au 4f:Si 2p(Si − O) ratio (squares), and N 1s:Si 2p(Si − O) ratio (circles) both show a linear increase in signal with layer number. Each data point represents the average of data collected from four samples, and the data are presented with layer 0 as the APTES-functionalized silicon substrate.

PDDA layers. This observation is also reflected in our ellipsometric data (Figure 4b below).

Because the refractive indices of such nanoparticle/polyelectrolyte composites are not known, we used spectroscopic multiangle ellipsometry to determine the real and imaginary refractive index values for such composite films.

The optical modeling was carried out in several stages. First, the optical properties of a cleaned bare silicon substrate were measured as a function of wavelength between 400 and 750 nm and at several angles of incidence, namely, 65°, 70°, and 75°. The silicon was assumed to be of semi-infinite thickness, and its optical parameters were determined through evaluation of the experimental data. Once these parameters had been determined, an APTES layer was added, and the refractive index modeled using the Cauchy expression for a normal dispersion (eq 7) with the assumption that the refractive index has only a nonzero real component.

$$n(\lambda) = A + \frac{B}{\lambda^2} + \frac{C}{\lambda^4} \tag{7}$$

The best fit occurred for $A = 1.45$, $B = 0.01$, and $C = 0$.

The model was completed by the addition of a nanoparticle/polyelectrolyte layer. It should be noted that, in approximating the film as a homogeneous system, we are combining the optical properties of the nanoparticles (including their stabilizing ligand), the polyelectrolyte, and any voids between. The nanoparticle/polyelectrolyte layer was simulated optically with a Lorentz oscillator model (eq 8).[30]

$$\tilde{\epsilon}(h\nu) = \epsilon_{1\infty} + \sum_m \frac{A_m}{E_m{}^2 - (h\nu)^2 - \mathrm{i}B_m h\nu} \tag{8}$$

In this equation, A_m is the amplitude, E_m is the center energy, and B_m is the broadening for the mth oscillator. For simplicity, we assume the system to be represented by a two-oscillator system with one oscillator to represent the background contribution and the other for the plasmon absorption band associated with the nanoparticles.

Figure 4a shows the n and k values determined from the fitting of the variable-angle ellipsometric data. The value for the refractive index of the Au:COOH/PDDA film at 633 nm was found from the graph in Figure 4a to be $k = 0.25$ for $n = 1.74$. These values are very different from those found by Brust et al.[15,36] and Auer et al.[37] However, their work was performed with films of nanoparticles linked by short-chain molecules, and therefore, their films had a much higher nanoparticle density. The polyelectrolyte PDDA alone would be expected to have a value of n close to 1.5 at this wavelength. Thus, our values appear to represent some kind of composite whose real

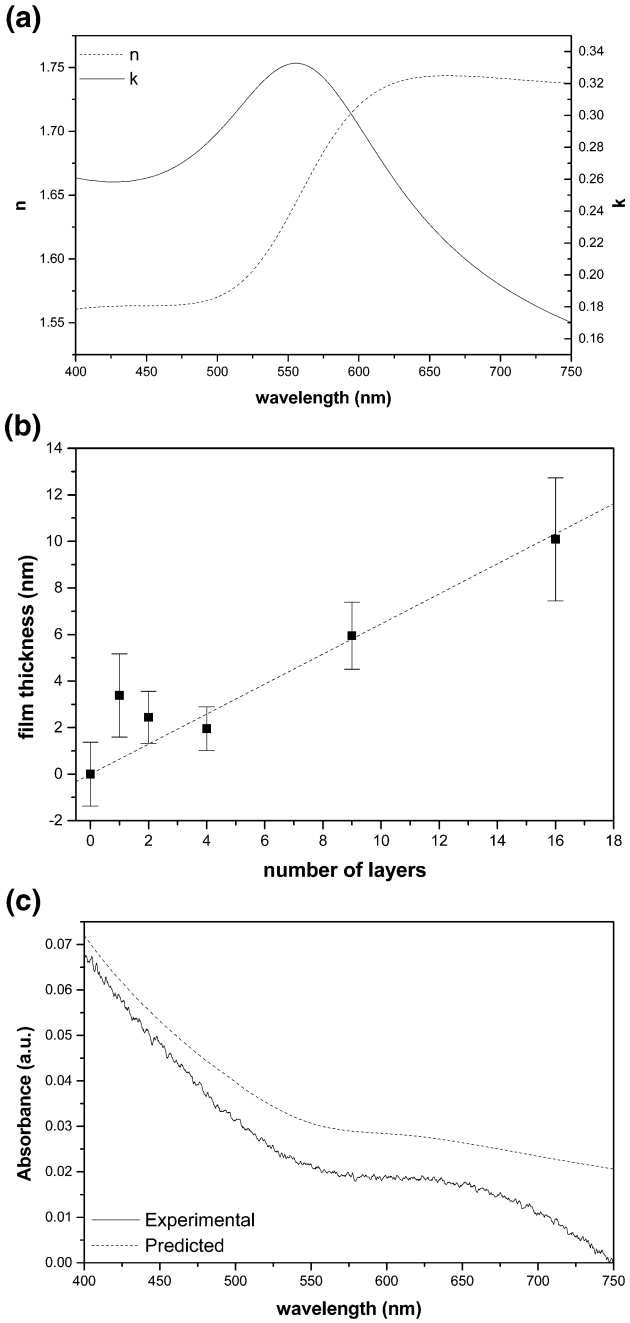

Figure 4. (a) n and k values as a function of wavelength calculated ellipsometrically. (b) Film thickness as a function of the number of layers as determined from the refractive indices in part a. Each point in this figure represents the average of data collected from four samples. The base layer is taken as APTES-functionalized silicon, layer 1 and subsequent odd-numbered layers correspond to the deposition of Au:COOH nanoparticles, and layer 2 and subsequent even-numbered layers correspond to the deposition of PDDA. (c) Simulated (based on n and k values given in part a) and experimental (from a 16-layer sample on APTES-functionalized silicon) UV/visible absorption spectra in reflection mode.

component is largely dominated by the polyelectrolyte into which metallic cores are dispersed.

Using the n and k values determined above, we calculated the average thickness increase per bilayer to be approximately 1.3 nm, as shown in Figure 4b. This value is significantly lower than we would expect given the dimensions of the nanoparticles and suggests that low surface coverage was attained.

In fitting our experimental data, we made several assumptions. Specifically, we considered the nanoparticle/polyelectrolyte film to be homogeneous, that is, interdigitation of the layers was significant enough that no formal stratified structure was present. Such a picture is in agreement with that put forward in the literature through neutron reflectivity studies of polyelectrolyte multilayer films,[38] although nanoparticle/polyelectrolyte films are believed to contain slightly more structure.[11] The film was also assumed to have abrupt interfaces with the silane layer and at the air/film interface. As a test that the values for the optical constants of the Au:COOH/PDDA films found through the fitting of the ellipsometric data were physically sensible, these values were used to simulate the UV/visible spectra.[39] The simulated spectrum and experimental data (collected in reflection mode) for a 16-layer film are shown in Figure 4c and demonstrate reasonable correspondence.

Conclusion

Multilayer films containing gold nanoparticles (stabilized with a carboxylic acid terminated thiol) and the polyelectrolyte PDDA have been synthesized on APTES-functionalized silicon substrates. It is evident from the Kelvin probe measurements that the sign of the surface charge oscillates, as expected if layer formation is being driven by electrostatic interactions. Modeling of the results also indicates a band bending contribution to the CPD associated with the equilibration of the Fermi levels of the semiconductor substrate and the nanoparticle film. The results suggest that the nanoparticle film is behaving as a p-type semiconductor with an acceptor density of 4.4×10^{25} m^{-3}.

Ellipsometric measurements suggest that each "bilayer" is quite thin and, indeed, substantially thinner than expected for complete monolayer growth. This finding might be dependent on the conditions (e.g., pH) used during film growth. These results explain the poor conductivity found in these films. The refractive indices for the bulk nanoparticle/polyelectrolyte composite could be reasonably modeled using a Lorentzian oscillator model, and values for the refractive index as a function of wavelength were obtained.

Acknowledgment. We acknowledge EPSRC for their funding of this work. K.C. additionally acknowledges the receipt of an EPSRC CASE studentship with the Seiko Epson Corporation.

References and Notes

(1) Fendler, J. H. *Chem. Mater.* **1996**, *8*, 1616.
(2) Dorogi, M.; Gomez, J.; Osifchin, R.; Andres, R. P.; Reifenberger, R. *Phys. Rev. B* **1995**, *52*, 9071.
(3) Moore, R. G. C.; Evans, S. D.; Shen, T.; Hodson, C. E. C. *Physica E* **2001**, *9*, 253.
(4) Iler, R. K. *J. Colloid Interface Sci.* **1965**, *21*, 569.
(5) Decher, G. *Science* **1997**, *277*, 1232.
(6) Lvov, Y.; Ariga, K.; Ichinose, I.; Kunitake, T. *J. Chem. Soc., Chem. Commun.* **1995**, 2313.
(7) Takahagi, T.; Tsutsui, G.; Huang, S.; Sakaue, H.; Shingubara, S. *Jpn. J. Appl. Phys. 2: Lett.* **2001**, *40*, L521.
(8) Caruso, F.; Caruso, R. A.; Mohwald, H. *Science* **1998**, *282*, 1111.
(9) Lvov, Y.; Ariga, K.; Onda, M.; Ichinose, I.; Kunitake, T. *Langmuir* **1997**, *13*, 6195.
(10) Liu, Y. J.; Wang, A. B.; Claus, R. *J. Phys. Chem. B* **1997**, *101*, 1385.
(11) Kotov, N. A.; Dekany, I.; Fendler, J. H. *J. Phys. Chem.* **1995**, *99*, 13065.
(12) Dante, S.; Hou, Z. Z.; Risbud, S.; Stroeve, P. *Langmuir* **1999**, *15*, 2176.
(13) Liu, Y. J.; Wang, Y. X.; Claus, R. O. *Chem. Phys. Lett.* **1998**, *298*, 315.
(14) Wuelfing, W. P.; Zamborini, F. P.; Templeton, A. C.; Wen, X. G.; Yoon, H.; Murray, R. W. *Chem. Mater.* **2001**, *13*, 87.
(15) Brust, M.; Bethell, D.; Kiely, C. J.; Schiffrin, D. J. *Langmuir* **1998**, *14*, 5425.
(16) Hao, E. C.; Lian, T. Q. *Chem. Mater.* **2000**, *12*, 3392.
(17) Gao, M. Y.; Richter, B.; Kirstein, S.; Mohwald, H. *J. Phys. Chem. B* **1998**, *102*, 4096.
(18) Caruso, F.; Mohwald, H. *Langmuir* **1999**, *15*, 8276.
(19) Ladam, G.; Schaad, P.; Voegel, J. C.; Schaaf, P.; Decher, G.; Cuisinier, F. *Langmuir* **2000**, *16*, 1249.
(20) Li, L. S.; Wang, R.; Fitzsimmons, M.; Li, D. Q. *J. Phys. Chem. B* **2000**, *104*, 11195.
(21) Li, L. S.; Li, A. D. Q. *J. Phys. Chem. B* **2001**, *105*, 10022.
(22) Li, L. S.; Jia, Q. X.; Li, A. D. Q. *Chem. Mater.* **2002**, *14*, 1159.
(23) Johnson, S. R.; Evans, S. D.; Brydson, R. *Langmuir* **1998**, *14*, 6639.
(24) Wei, Z. Q.; Wang, C.; Zhu, C. F.; Zhou, C. Q.; Xu, B.; Bai, C. L. *Surf. Sci.* **2000**, *459*, 401.
(25) Cant, N. E.; Critchley, K.; Zhang, H.-L.; Evans, S. D. *Thin Solid Films* **2003**, *426*, 31.
(26) Briggs, D.; Seah, M. P. *Practical Surface Analysis: Auger and X-ray Photoelectron Spectroscopy*, 2nd ed.; John Wiley & Sons: New York, 1996.
(27) Hammond, P. T.; Whitesides, G. M. *Macromolecules* **1995**, *28*, 7569.
(28) Tronin, A.; Lvov, Y.; Nicolini, C. *Colloid Polym. Sci.* **1994**, *272*, 1317.
(29) Tseng, J. Y.; Lin, M. H.; Chau, L. K. *Colloid Surf. A: Physicochem. Eng. Asp.* **2001**, *182*, 239.
(30) Lvov, Y. M.; Rusling, J. F.; Thomsen, D. L.; Papadimitrakopoulos, F.; Kawakami, T.; Kunitake, T. *Chem. Commun.* **1998**, 1229.
(31) Ung, T.; Liz-Marzan, L. M.; Mulvaney, P. *J. Phys. Chem. B* **2001**, *105*, 3441.
(32) Schroder, D. K. *Meas. Sci. Technol.* **2001**, *12*, R16.
(33) Sze, S. M. *Physics of Semiconductor Devices*, 2nd ed.; John Wiley & Sons: New York, 1981.
(34) Brennan, K. F. *The Physics of Semiconductors: With Applications to Optoelectronic Devices*; Cambridge University Press: Cambridge, U.K., 1999.
(35) Lvov, Y.; Decher, G.; Mohwald, H. *Langmuir* **1993**, *9*, 481.
(36) Baum, T.; Bethell, D.; Brust, M.; Schiffrin, D. J. *Langmuir* **1999**, *15*, 866.
(37) Auer, F.; Scotti, M.; Ulman, A.; Jordan, R.; Sellergren, B.; Garno, J.; Liu, G. Y. *Langmuir* **2000**, *16*, 7554.
(38) Korneev, D.; Lvov, Y.; Decher, G.; Schmitt, J.; Yaradaikin, S. *Physica B* **1995**, *213*, 954.
(39) Heavens, O. S. *Optical Properties of Thin Solid Films*; Butterworth Scientific: London, 1955.